Anomalous binding memory in heterogeneous molecular systems

Shiyi Qin[1,†,*], Fangxuan Lyu[1,†], Xuebo Quan[1], Bing Miao[2], Kai Huang[1,*]

[1]Institute of Systems and Physical Biology, Shenzhen Bay Laboratory, Shenzhen, 518107, China

[2]Center of Materials Science and Optoelectronics Engineering, College of Materials Science and Opto-Electronic Technology, University of Chinese Academy of Sciences (UCAS), Beijing 100049, China

[†]These authors contribute equally

*Correspondence: qinsy@szbl.ac.cn (S.Q.), huangkai@szbl.ac.cn (K.H.)

Abstract: Understanding how molecular binding couples with diffusion is fundamental to molecular engineering and biomedical applications. At the mesoscale, this coupling gives rise to a binding memory effect, characterized by power-law decays in temporal binding autocorrelations. This repeated binding-unbinding cycles transforms the static, affinity-limited binding picture into a dynamic landscape. While scaling theory has successfully described simple systems, the nature of this coupling in realistic, heterogeneous environments remains poorly understood. Here, we combine high-throughput simulations, theoretical analysis and numerical modelling to reveal how environmental heterogeneity reshapes binding memory and transport statistics. We show that hopping, a nonlocal jump process, induces strong spatiotemporal correlations across binding sites. This leads to diffusion with non-Gaussian statistics and a spectrum of anomalous scaling behaviors for binding memory. In contrast to the universal scaling observed in homogeneous settings, the complex binding-diffusion interplay in heterogeneous binding landscape renders binding memory a tunable property, opening new avenues for molecular-level engineering of chemical reactions, catalysis, and materials design.

Significance

At the mesoscale, the processes of binding and diffusion are intrinsically coupled. Spatial heterogeneity, a ubiquitous feature of natural systems, profoundly complicates this interplay, yet its functional consequences remain elusive. Through integrated multiscale simulations, theoretical analysis, and numerical modeling, we uncover an anomalous binding memory effect in heterogeneous landscapes, driven by non-local molecular hopping. This effect is characterized by a power-law decay in the binding autocorrelation function. In contrast to the fixed scaling observed in homogeneous environments, the scaling exponent in heterogeneous systems is tunable by modulating molecular hopping dynamics or by engineering the spatial patterning of the heterogeneity itself. Our work thus establishes a bridge between fundamental physical principles, complex biological phenomena, and programmable materials design.

Introduction

Molecular systems, from enzymes (1–3) in living cells to transcription factors locating their DNA target sites (4–6), operate across multiple length and time scales,

with their dynamics primarily governed by two fundamental processes, spatial exploration (diffusion) and specific recognition (binding). At macroscopic scales, molecular motion appears as a continuous diffusive field, where the rapid contacts between individual molecules are averaged out and effectively invisible. Zooming to the single-molecule level allows for detailed observation of how a molecule selectively binds to its target, a process governed by the local energy landscape and thermal fluctuations. Bridging these extremes is the mesoscale, where molecules reach beyond their local area, sense distant partners, and form spatial correlations across regions. Diffusion paths are no longer passive trajectories but couple distinct binding events.

Studying this cross-scale interplay necessitates experimental techniques that simultaneously resolve transient binding and track long-term trajectories. This dual requirement, however, confronts a longstanding trade-off between spatiotemporal resolution and observation duration in methods like single-molecule tracking (SMT) (7, 8). Theoretically modeling these non-local, coupled dynamics is equally challenging, as it requires explicit consideration of complex many-body effects. Several phenomenological approaches, including reaction-diffusion models, address part of this complexity by treating molecular populations as continuum fields and coupling bulk diffusion to binding via mean-field exchange rates (9–11). However, these frameworks inherently overlook fluctuations at the single-molecule level, even though such fluctuations often drive biological function (12). For example, gene transcription can be initiated by a transient spike in transcription factor occupancy that crosses a high activation threshold (13, 14). In this way, biological systems leverage large fluctuations, rather than just population averages, to trigger decisive, irreversible responses. Deciphering binding-diffusion coupling at the single-molecule level is thus necessary to uncover the physical mechanisms of living systems.

Our previous work addressed this challenge though an integrated methodology, combing active-feedback SMT experiment, scaling theory and simulations. We revealed that the intrinsic coupling between binding and diffusion creates a binding memory (15). It manifested as a power-law decay in the binding autocorrelation function (BAF), defined as

$$BAF(\Delta t) = \frac{\sum_{t=0}^{T-\Delta t} n(t)n(t+\Delta t)}{\sum_{t=0}^{T-\Delta t} n(t)^2}$$

where $n(t)$ denote the number of bound molecules at time t, and $n(t+\Delta t)$ is the number of those pairs remaining bound or rebinding after lag time Δt. The non-exponential kinetics suggests a new paradigm in which binding specificity can emerge from the cumulative effect of repeated weak interactions, rather than a single strong binding event (16–18). However, these investigations have largely focused on simple, homogeneous systems where binding events are weakly correlated. In reality, heterogeneous energy landscapes in biological and functional materials create history-dependent binding with strong correlations. This spatial heterogeneity, when coupled with the binding-diffusion interplay, presents a dual complexity. A central question thus emerges: what is the nature of binding memory in such a complex regime?

To bridge this gap, we introduce a bottom-up multiscale simulation framework integrating large-scale all-atom molecular dynamics with Langevin dynamics. Leveraging over 5×10^6 core-hours of computation across an extensive range of systems, we systematically investigate how spatial heterogeneity, diffusion dimensionality, the nature of binding forces (e.g., isotropic versus directional), and physicochemical properties of the environment (e.g., viscosity and crowding) collectively dictate the emergence and strength of molecular binding memory. Our simulations reveal a rich, tunable spectrum of anomalous BAF scaling, distinct from the fixed exponent observed in homogeneous systems. These emergent behaviors share a common microscopic origin: non-Gaussian displacement statistics arising from spatially non-local molecular hopping. For heterogeneities arranged in well-defined geometries, we derive the limiting BAF scaling analytically. Building on this physical picture, we further show that engineered binding landscapes enable programmable control of binding memory. This work establishes binding-diffusion coupling as a fundamental principle governing molecular specificity and transport in heterogenous environments, with broad implications for designing functional materials.

Breakdown of universal BAF scaling in heterogeneous binding systems

We begin our exploration of coupled molecular transport and binding in 3D heterogeneous environments. A classic example is the interaction between chromatin and trans-acting factors (TAFs). Chromatin, with its hierarchical organization and sequence-dependent binding heterogeneity presents a complex landscape for TAFs (e.g., transcription factors or chromatin remodelers) to navigate and bind (19–21). In our coarse-grained simulation framework, chromatin is represented as a 3D polymer chain with specific binding sites ($\epsilon = 1.6$) distributed randomly along its contour. TAFs are modeled as diffusing polymers subject to Langevin dynamics. To mimic crowded intracellular environments, we introduce inert crowders at varying concentrations.

As a baseline, we first consider a homogeneous reference case with only nonspecific interactions (Fig. 1A). In this setting, the scaling exponent of the BAF remains fixed at -1.5, independent of the crowding level. This value is in line with the theoretical prediction D/θ, for the case of normal diffusion ($\theta = 2$) embedded in a three-dimensional space (D=3). In contrast, the amplitude of the BAF is modulated by the crowding.

Introducing a sparse distribution of specific binding sites imposes spatial heterogeneity, which we initially expected to disrupt the power-law behavior of BAF. Surprisingly, our simulations revealed that the power-law scaling persists. However, unlike the homogeneous case, the heterogeneous system exhibits a broad, crowding-dependent spectrum of exponents, all of which consistently deviate from the homogeneous reference value. To decipher the underlying mechanism, we analyzed single-molecule trajectories (Fig. 1D), which reveal frequent, long-range hops between binding sites. These jumps induce path discontinuities, characteristic of a Lévy process, different from the Brownian motion in homogeneous systems (Fig. S1). The

displacement probability density function (PDF) accordingly becomes strongly non-Gaussian (Fig.1E), which implies the breakdown of scaling theories predicated on trajectory homogeneity. For a system with fixed dimensionality, the steeper BAF decay would be interpreted within the original framework as evidence for anomalous diffusion. This interpretation is, however, inconsistent with our mean-squared displacement (MSD) analysis (Fig. S2), which shows normal diffusion. We therefore conclude that the faster BAF decay stems not from super-diffusion, but from the dynamic heterogeneity inherent to the intermittent hopping process. This anomalous BAF scaling is an emergent, non-asymptotic phenomenon manifesting in an intermediate time window, where transport couples with binding heterogeneity to generate non-Gaussian dynamics. At longer times, as the system fully samples the heterogeneity, these coupling-induced non-Gaussian effects decay, and the scaling crossovers back to the homogeneous exponent of -1.5 (see Fig. S3).

To further understand how crowding regulates the BAF scaling, we performed a statistical analysis of hop lengths across a range of crowding conditions (see Fig. 1D & Fig. S4). Our results reveal a strong correlation between the scaling exponent and hopping capability. Increased diffusion rates facilitate longer-range jumps, allowing molecules to reach distal binding sites and reducing rebinding to nearby traps. Conversely, crowding slows diffusion, thereby confining molecular search to the local environment and strongly promoting immediate rebinding.

Heterogeneity in binding environments often extends beyond a complex affinity landscape. Phase separation has emerged as a key and widespread mechanism for generating spatial complexity, as frequently observed in living systems (22–24). This process drives proteins to demix from the surrounding milieu, forming dense, liquid-like condensates with physicochemical properties different from the dilute phase. To capture the protein dynamics within this multi-phase setting, we build a minimal computational model (Fig. 1F) where phase-separating proteins are represented as homopolymers with attractive interactions. At concentrations above the critical saturation threshold, droplets are spontaneously formed, coexisting with a dilute surrounding phase. We observe dynamic molecular exchange between these phases, and interestingly, the spatiotemporal heterogeneity of leaving and rebinding at the droplet interface can still be described by a power-law dependence. Through in silico adjustments of solvent viscosity (Fig. 1H), we further reveal that the material properties of the microenvironment do not only simply influence the molecular mobility, but also dynamically fine-tune the mesoscopic scaling laws. This dependence is fundamentally different from the trivial scaling behavior observed in single-phase systems. The insights gained from these two representative types of 3D heterogeneous binding systems may offer broader relevance and could potentially inform our understanding of other soft and biological matter systems, such as porous nanomaterials, mixed polyelectrolyte solutions, and colloidal gels.

In homogeneous binding systems, we have already observed a stark contrast between the BAF and the distribution of continuous binding lifetime distribution (LDF). We revisit the LDF in heterogeneous environments with more complex energy landscapes (Fig. S5). Here, our calculations reveal that the LDF still deviate from

power-law and decays rapidly to negligible level. It suggests that binding memory, rather than static binding affinity, is the key factor in extending effective interactions.

Binding dynamics in low-dimensional heterogenous systems

Many fundamental biological processes unfold within low-dimensional landscapes. These include protein-lipid interactions on two-dimensional cell membranes (25), the transport of regulatory molecules (e.g., transcription factors and enzymes) within the fractal confines of chromatin (26, 27), and the one-dimensional motions such as TFs sliding along DNA (28) or cohesin-mediated DNA loop extrusion (29, 30). Moreover, these low-dimensional environments are inherently disordered. Biomembranes feature non-uniform chemical compositions and physical structures, while the chromatin fiber, as a 1D path, has a convoluted energy landscape shaped by its higher-order folding structures and sequence-dependent affinities.

To investigate binding dynamics in low-dimensional heterogeneous systems, we constructed a set of minimal computational models. Specifically, we simulated adsorbate molecules interacting with a 2D membrane, polymers confined within a fractal scaffold (D=1.7) generated via diffusion-limited aggregation (31, 32), and a ring-polymer sliding on a quasi-one-dimensional chromatin polymer. Heterogeneity was achieved through the random placement of specific binding sites within the topological space of each system. Homogeneous controls for these models (Fig. S6) showed insensitivity of BAF to diffusivity, with power-law exponents (-1.0, -0.62, -0.45) governed purely by system dimensionality. In striking contrast, heterogeneous systems retained power-law behavior but, more significantly, displayed a rich spectrum of anomalous exponents that could be dynamically tuned by the diffusive properties of the environment. Analysis of single-molecule trajectories (Fig. S7) further revealed universal features across dimensions, including sporadic trapping/release events and non-Gaussian dynamics (Fig. S8). These results, together with our 3D findings, establish that the non-Gaussian dynamics and emergent scaling from binding-diffusion coupling are a universal, dimensionality-robust phenomenon.

In heterogeneous systems, molecular hopping typically weakens binding memory, reducing the BAF exponent below the homogeneous benchmark of -1.0. Paradoxically, we have uncovered a counteracting regime (boosting BAF scaling above -1.0) in our 2D system where high binding-site density combined with suppressed diffusion gives rise to a caging effect. Here, molecules become dynamically confined by the densely packed traps, which prevents long-range escape and restricts their motion to localized, back-and-forth dynamics around their original sites. This dramatically enhances rebinding and consequently strengthens binding memory. The generality of this caging effect is confirmed in a fractal system (Fig. S9A). Such bidirectional tunability of binding memory broadens the potential application space.

We now turn to the case of a zero-dimensional (D=0) system, an extreme case of low-dimensional system. Unlike our previous analysis of 3D protein transport across droplets, here we focus on internal polymer dynamics within individual condensates. Using a system with strong phase-separating capability, we tightly confine the polymer within a single droplet. This spatial confinement results in a BAF that approaches zero

(Fig. 2D), indicative of a quasi-0D environment on relevant timescales. However, introducing an additional component, such as scaffold proteins capable of interacting specifically with other proteins, shifts the BAF to -0.41. This demonstrates that the intrinsic compositional diversity of biomolecular condensates can generate a heterogeneous internal landscape, supporting dynamics far more complex than those in simplistic, single-component droplets. Moreover, such internal heterogeneity is not restricted to multi-component systems. Even within condensates of uniform composition, heterogeneity can arise from the coexistence of distinct protein states. One potential mechanism for this is the formation of a percolated network, which could create a spectrum of dynamic modes ranging from transient trapping to random diffusion-like motion, within a single condensate (33, 34).

Impact of binding nature on heterogeneous binding dynamics

Extending beyond isotropic interactions, we studied hydrogen-bond-mediated binding of water under nanoscale confinement including 2D graphene slits and 1D carbon nanotubes. While extensively studied, most previous work has considered idealized, homogeneous setups (35, 36). To move beyond this simplification, we use all-atom simulations to investigate the hydrogen-bond binding memory of water within spatially heterogeneous chemical landscapes. These are created by randomly functionalizing the confining surfaces with epoxy and hydroxyl groups, which act as specific hydrogen-bonding sites (Fig. 3A&D). Anomalous BAF scaling, deviating from ideal 1D and 2D cases, appears in our heterogeneous aqueous system as well, suggesting the universality of this phenomenon across different binding natures. In addition to calculating the hydrogen-bond autocorrelation (BAF_{HB}), we also computed the residence autocorrelation (RAF). This function tracks whether a water molecule is present within a 5Å radius of a binding site over time, analogous to the BAF in isotropic systems, where binding is solely dependent on spatial proximity. The BAF_{HB} exhibits a lower scaling exponent (Fig. 3B,C,E,F) relative to RAF. This stems from the fact that even if a water molecule revisits the spatial vicinity of a former binding site, rebinding is not guaranteed if those sites are already occupied. Such valency limitations lead to more complex, correlated dynamics that further reduce the scaling exponent. Another key difference from our earlier models is the use of an explicit solvent description, which naturally includes hydrodynamics. The consistency of these anomalous scaling laws is particularly notable given that this system incorporates directional interactions and explicit hydrodynamics features absent in our coarse-grained model. It reinforces the robustness of the binding-diffusion coupling phenomenon and rules out possible artifacts from implicit solvent approximations. These insights have implications for the development of functional nanomaterials where adaptable water transport is essential, such as selective nanofiltration membranes and nanofluidic ion circuits.

Interfacial effects in heterogenous systems of mixed dimensionalities

So far, we have focused on systems with binding sites randomly dispersed throughout the entire space. We now turn to a more intriguing class of heterogeneity where binding sites are confined to sub-domains that are geometrically distinct from

the embedding diffusion space, forming mixed-dimensional systems. We ask the question: how does such spatially compartmentalized heterogeneity influence the behavior of binding memory? To address this, we construct three representative systems: a 2D binding surface within 3D space (2D+3D; Fig.4A), a 1D adsorption chain embedded in a 2D plane (1D+2D; Fig.4C), and a 1D chain in 3D space (1D+3D; Fig.4E). Their BAF scaling exponents, measured as -2.4, -1.95, and -1.70 (Fig. 4B,D,F), lying far outside the predicted range for homogeneous systems (-1.0 and -1.5). This consistent anomaly originates from heterogeneity-induced non-Gaussian dynamics, as confirmed in Fig. 4B, D, F.

To decipher the physics of 2D+3D and 1D+2D cases, we developed a simplified theoretical model (see ***Supporting Information*** for details). The geometric nature of the heterogeneity in these systems allows for a well-defined adsorption boundary condition, which we treat as perfectly absorbing. Using the method of images, this model predicts rebinding probability of $P_{rebind} \sim t^{-2.5}$ and $P_{rebind} \sim t^{-2.0}$, respectively. These analytical results align closely with our simulation measurements, though slightly lower due to the model's idealization of a single, non-return hopping event, which represents a theoretical limiting case equivalent to a hop of infinite length. In practice, a molecule undergoes a series of finite-length hops that keep it within the vicinity of its original binding site, allowing for repeated rebinding opportunities. Our use of a relatively fast diffusion setting promotes longer hops, thus minimizing such returns and narrowing the gap between simulation and the theoretical limit. This model is particularly useful for predicting the asymptotic behavior in such heterogeneous distributions, yielding a universal scaling: $BAF \sim t^{-\frac{D}{2}-1}$ with D and D-1 being the dimensionalities of the diffusion space and the heterogeneity, respectively.

The scaling law summarized previously applies to systems with a one-dimensional difference between the heterogeneity and diffusion spaces. An interesting extension is to a two-dimensional gap, as in 1D+3D system, where analytical tractability is challenging. We therefore determined the corresponding scaling limit numerically (further details in ***Supporting Information***). As shown in Fig. S11, the resulting limit agrees well with our simulation results presented in Fig. 4F. We now place this result in a broader context by comparing it to other 3D systems with distinct heterogeneity patterns, such as binding sites confined to a 2D plane or randomly dispersed in 3D space. A clear hierarchy emerges: the 3D+3D system displays the steepest scaling, followed by the 2D+3D and then the 1D+3D systems. This trend highlights that the dimensionality of spatial heterogeneity (i.e., spatial architecture of heterogeneity) is a key determinant of molecular binding memory. It determines the level of disruption to spatial homogeneity from minimal perturbation by a 1D line to a fully disordered 3D arrangement.

Molecular binding memory in heterogenous systems with binding gradient

Building on the role of heterogeneous distributions, we next ask how asymmetric patterns, common in non-equilibrium systems, influence binding memory. For this purpose, we designed a 2D membrane featuring six adjacent regions with a stepwise

increase in densities of binding sites (see Fig. 5A), creating a continuous binding gradient. This design generated strong inter-region binding correlations, causing BAF scaling in the gradient-connected setup to deviate sharply from that in isolated counterparts (see Fig. 5E). Notably, it induced a pronounced spatially polarized binding memory. In the highest-density region, BAF values exceeded -1.0 (Fig. 5D), reflecting robust binding memory that promotes stable attachments, while the sparsest regions dropped to BAF=-2.25 (Fig. 5C), indicating weak memory that favors molecular turnover. Unlike our static gradient, real biological systems often shape their heterogeneous binding landscapes through dynamic, temporally evolving processes, yielding context-dependent memory to support function. For example, when a virus or signaling ligand bind to a membrane, it can trigger local receptor clustering and recruitment of downstream effectors (37–39). This converts a temporal sequence of binding events into persistent spatial heterogeneity, such as density gradients or functional domains. The resulting heterogeneity, in turn, preferentially direct subsequent binding events to these enriched regions, revealing a strong memory. Even in our minimal 2D gradient pattern, binding memory is inherently spatiotemporally entangled. Scaling up to more complex higher-dimensional patterns or to real non-equilibrium systems with dynamically evolving patterns, would enable more sophisticated binding-memory networks, pointing to a potential direction for engineering functional biomaterials.

Discussions

Our work, supported by extensive simulations, has discovered a rich spectrum of anomalous BAF scaling laws in multidimensional heterogeneous systems, which stands in sharp contrast to homogeneous environments. Non-local hopping events spatiotemporally couples the binding pathways of different molecules and induces non-Gaussian dynamics. For heterogeneities confined to well-defined geometries, we combined simulations and theoretical analysis to confirm the robustness of these anomalous scalings and derive their asymptotic limits. Finally, by engineering binding patterns with asymmetry that mimic non-equilibrium systems, we show that binding memory becomes context-sensitive, pointing to this being an intrinsic property under non-equilibrium conditions.

Based on our findings, we propose some new perspectives on several fundamental problems. First, we expand the concept of molecular specificity beyond static binding affinity. We demonstrate that the local environment flexibly tunes binding memory, thereby establishing specificity as a dynamic and context-dependent property where the environment serves as an additional control layer. Second, many biological models overlook heterogeneity-driven non-Gaussian dynamics. For instance, the classic transcription factor search is often simplified as a 1D/3D switch, ignoring the inherent heterogeneity of chromatin and nuclear space, a condition that produces non-Gaussian dynamics. Similarly, in biomolecular condensates, spatial heterogeneity is an intrinsic property. This arises from either the diversity of molecular interactions in multicomponent systems or the complex network structures in single-component condensates (33). Such heterogeneity manifests as a spectrum of transient dynamical

states. While often reflected in anomalous diffusion, it can also lead to complex phenomena like "Fickian yet non-Gaussian" diffusion (40). Consequently, these dynamic signatures are averaged out in ensemble measurements. Direct observation of the underlying inhomogeneous kinetics therefore necessitates a single-molecule perspective, which spatially and temporally resolves individual molecular behaviors. Finally, our research holds significant implications for material processing. Heterogeneity can be harnessed to precisely modulate binding memory at the single-molecule level, thereby influencing the overall material properties and functions. Our work thus establishes a bridge connecting fundamental physical phenomena with complex biological processes and cutting-edge material design.

Our current research is limited by the use of a static, "frozen" designed binding landscape. It is a necessary simplification that isolates the effect of the heterogeneity pattern from temporal fluctuations, allowing us to establish clear relationships between spatial heterogeneity, topological dimensions, and binding memory. This approximation is physically justified by the widespread phenomenon of timescale separation in biological systems. Specifically, the processes that establish heterogeneous structures (e.g., chromatin looping, condensate formation) often evolve over seconds to minutes, far slower than the microsecond to millisecond binding/dissociation dynamics we study.

In our future work, we will explore a more realistic and complex scenario: a dynamically fluctuating energy landscape. We hypothesize that living systems not only utilize static spatial heterogeneity to encode information but also achieve dynamic editing of molecular binding memory by precisely regulating the temporal dynamics of these heterogeneities.

Methods

Multi-scale simulation framework

We employed a multi-scale computational approach that integrates coarse-grained molecular simulations for the physical reconstruction of complex biological systems, all-atom studies of confined water, and engineered systems with designed heterogeneous patterns. This allowed us to systematically investigate molecular binding and diffusion across a wide spectrum of spatially heterogeneous environments.

The specific systems modeled include: (1) protein polymers interacting with chromatin fibers and liquid-liquid phase separation (LLPS) droplets; (2) binding dynamics of particles in 2D-confined substrate and fractal DLA scaffolds; (3) sliding of a ring polymer topologically constrained to a chromatin fiber; (4) the dynamics of protein polymers confined within LLPS droplets; and (5) all-atom molecular dynamics of water under 1D and 2D confinement.

Coarse-grained simulations utilized Langevin dynamics with specific and non-specific interactions tuned via Lennard-Jones potentials. All-atom water simulations employed the SPC/E model with the OPLS-AA force field for carbon nanomaterials, using the GROMACS package (42). All systems were custom-built. Full construction protocols, parameters, and the simulation code are detailed in ***Supporting Information*** and have been archived on GitHub (https://github.com/sqin5/binding-memory).

Analyses of binding dynamics

To characterize binding memory, we defined a binding time autocorrelation function, Binding events were identified at every sampling frame based on either a distance-based or a hydrogen-bonding criterion. Capturing the rapid decay of temporal correlations required high-frequency sampling and robust statistical averaging, which we achieved by running multiple independent replicas of large-scale simulations. This procedure generated large datasets of molecular binding events, making their post-processing a severe computational bottleneck with conventional analysis methods.

The computational challenge centered on constructing the intermolecular contact matrix at each sampling timestep. Conventional methods that store the full matrix of all molecular pairs are highly inefficient for sparse, transient interactions, as they waste significant memory and computational resources on zero entries. We addressed this by implementing a hashmap-based data structure that recorded only active molecular pairs. Each interacting pair was stored as a unique key (e.g., "*i_j*") mapped to a Boolean binding state. This sparse representation significantly reduced memory usage, enabled constant-time state lookup, and dramatically accelerated the temporal comparison of contact matrices required for BAF calculation. The analysis code was further parallelized using OpenMP. All custom analysis tools and the modified LAMMPS (42) version are available on Github (https://github.com/sqin5/binding-memory).

Acknowledgements

This work was funded by grants from the Major Program of Shenzhen Bay Laboratory (grant no. S241101001 to K.H.), National Natural Science Foundation of China (grant no. 32571445 and no. 32521002 to K.H., grant no. 22403068 to S.Q.), the Shenzhen Bay Laboratory Open Fund Project (grant no. SZBL2021080601013 to K.H.). We acknowledge computational support from the Shenzhen Bay Laboratory High Performance Computing and Informatics Core.

Contributions

K.H. and S.Q. conceived, guided and supervised the project; S.Q., F. L. and X.Q. designed and performed computer simulations; S.Q., K.H. and B.M. formulated the theoretical framework of the manuscript. S.Q. and K.H. wrote the manuscript. All authors discussed the results and reviewed the manuscript.

Competing Interest Statement

The author declares no competing interest

References

1. E. J. Jervis, C. A. Haynes, D. G. Kilburn, Surface Diffusion of Cellulases and Their Isolated Binding Domains on Cellulose. *Journal of Biological Chemistry* **272**, 24016–24023 (1997).
2. I. V. Gopich, A. Szabo, Diffusion modifies the connectivity of kinetic schemes for multisite binding and catalysis. *Proc. Natl. Acad. Sci. U.S.A.* **110**, 19784–19789 (2013).

3. G. Giunta, H. Seyed-Allaei, U. Gerland, Cross-diffusion induced patterns for a single-step enzymatic reaction. *Commun Phys* **3**, 167 (2020).
4. J. Elf, G.-W. Li, X. S. Xie, Probing Transcription Factor Dynamics at the Single-Molecule Level in a Living Cell. *Science* **316**, 1191–1194 (2007).
5. J. Gorman, *et al.*, Single-molecule imaging reveals target-search mechanisms during DNA mismatch repair. *Proc. Natl. Acad. Sci. U.S.A.* **109** (2012).
6. X. A. Feng, *et al.*, GAGA zinc finger transcription factor searches chromatin by 1D–3D facilitated diffusion. *Nat Struct Mol Biol* **32**, 2359–2370 (2025).
7. A. A. Deniz, S. Mukhopadhyay, E. A. Lemke, Single-molecule biophysics: at the interface of biology, physics and chemistry. *J. R. Soc. Interface.* **5**, 15–45 (2008).
8. S. Hou, J. Exell, K. Welsher, Real-time 3D single molecule tracking. *Nat Commun* **11**, 3607 (2020).
9. A. V. Chechkin, I. M. Zaid, M. A. Lomholt, I. M. Sokolov, R. Metzler, Bulk-mediated diffusion on a planar surface: Full solution. *Phys. Rev. E* **86**, 041101 (2012).
10. D. Shoup, A. Szabo, Role of diffusion in ligand binding to macromolecules and cell-bound receptors. *Biophysical Journal* **40**, 33–39 (1982).
11. M. Kang, C. A. Day, E. DiBenedetto, A. K. Kenworthy, A Quantitative Approach to Analyze Binding Diffusion Kinetics by Confocal FRAP. *Biophysical Journal* **99**, 2737–2747 (2010).
12. L. Ham, M. A. Coomer, K. Öcal, R. Grima, M. P. H. Stumpf, A stochastic vs deterministic perspective on the timing of cellular events. *Nat Commun* **15**, 5286 (2024).
13. C. C.-S. Hsiung, *et al.*, A hyperactive transcriptional state marks genome reactivation at the mitosis–G1 transition. *Genes Dev.* **30**, 1423–1439 (2016).
14. N. Yosef, A. Regev, Impulse Control: Temporal Dynamics in Gene Transcription. *Cell* **144**, 886–896 (2011).
15. S. Qin, *et al.*, Binding memory of liquid molecules. *Nat Commun* **16**, 6555 (2025).
16. K. Aoki, M. Yamada, K. Kunida, S. Yasuda, M. Matsuda, Processive phosphorylation of ERK MAP kinase in mammalian cells. *Proc. Natl. Acad. Sci. U.S.A.* **108**, 12675–12680 (2011).
17. E. Arranz-Plaza, A. S. Tracy, A. Siriwardena, J. M. Pierce, G.-J. Boons, High-Avidity, Low-Affinity Multivalent Interactions and the Block to Polyspermy in *Xenopus l aevis*. *J. Am. Chem. Soc.* **124**, 13035–13046 (2002).
18. W. Pomp, J. V. W. Meeussen, T. L. Lenstra, Transcription factor exchange enables prolonged transcriptional bursts. *Molecular Cell* **84**, 1036-1048.e9 (2024).
19. K. S. Zaret, J. S. Carroll, Pioneer transcription factors: establishing competence for gene expression. *Genes Dev.* **25**, 2227–2241 (2011).
20. J. F. Kribelbauer-Swietek, *et al.*, Context transcription factors establish cooperative environments and mediate enhancer communication. *Nat Genet* **56**, 2199–2212 (2024).
21. S. A. Lambert, *et al.*, The Human Transcription Factors. *Cell* **172**, 650–665 (2018).

22. M. Feric, *et al.*, Coexisting Liquid Phases Underlie Nucleolar Subcompartments. *Cell* **165**, 1686–1697 (2016).
23. C. P. Brangwynne, *et al.*, Germline P Granules Are Liquid Droplets That Localize by Controlled Dissolution/Condensation. *Science* **324**, 1729–1732 (2009).
24. D. S. W. Lee, *et al.*, Size distributions of intracellular condensates reflect competition between coalescence and nucleation. *Nat. Phys.* **19**, 586–596 (2023).
25. T. Sych, K. R. Levental, E. Sezgin, Lipid–Protein Interactions in Plasma Membrane Organization and Function. *Annu. Rev. Biophys.* **51**, 135–156 (2022).
26. B. Meyer, O. Bénichou, Y. Kafri, R. Voituriez, Geometry-Induced Bursting Dynamics in Gene Expression. *Biophysical Journal* **102**, 2186–2191 (2012).
27. Y. Kim, L. Lizana, J.-H. Jeon, Fractal and Knot-Free Chromosomes Facilitate Nucleoplasmic Transport. *Phys. Rev. Lett.* **128**, 038101 (2022).
28. E. G. Marklund, *et al.*, Transcription-factor binding and sliding on DNA studied using micro- and macroscopic models. *Proc. Natl. Acad. Sci. U.S.A.* **110**, 19796–19801 (2013).
29. G. Fudenberg, *et al.*, Formation of Chromosomal Domains by Loop Extrusion. *Cell Reports* **15**, 2038–2049 (2016).
30. H. Zhao, *et al.*, Extensive mutual influences of SMC complexes shape 3D genome folding. *Nature* **640**, 543–553 (2025).
31. D. Liu, W. Zhou, X. Song, Z. Qiu, Fractal Simulation of Flocculation Processes Using a Diffusion-Limited Aggregation Model. *Fractal Fract* **1**, 12 (2017).
32. J. M. Tenti, S. N. Hernández Guiance, I. M. Irurzun, Fractal dimension of diffusion-limited aggregation clusters grown on spherical surfaces. *Phys. Rev. E* **103**, 012138 (2021).
33. Z. Shen, *et al.*, Biological condensates form percolated networks with molecular motion properties distinctly different from dilute solutions. *eLife* **12**, e81907 (2023).
34. S. Zhu, *et al.*, Demixing is a default process for biological condensates formed via phase separation. *Science* **384**, 920–928 (2024).
35. L. S. Moreira, D. D. De Vargas, M. H. Köhler, Modeling water transport properties in carbon nanotubes: Interplay between force-field flexibility and geometrical parameters. *Phys. Rev. E* **108**, 034116 (2023).
36. Z. Wan, *et al.*, Anomalous water transport in narrow-diameter carbon nanotubes. *Proc. Natl. Acad. Sci. U.S.A.* **119**, e2211348119 (2022).
37. P.-Y. Lozach, *et al.*, DC-SIGN as a Receptor for Phleboviruses. *Cell Host & Microbe* **10**, 75–88 (2011).
38. R. A. Villanueva, Y. Rouillé, J. Dubuisson, “Interactions Between Virus Proteins and Host Cell Membranes During the Viral Life Cycle” in *International Review of Cytology*, (Elsevier, 2005), pp. 171–244.
39. S. Boulant, M. Stanifer, P.-Y. Lozach, Dynamics of Virus-Receptor Interactions in Virus Binding, Signaling, and Endocytosis. *Viruses* **7**, 2794–2815 (2015).
40. B. Wang, J. Kuo, S. C. Bae, S. Granick, When Brownian diffusion is not Gaussian. *Nature Mater* **11**, 481–485 (2012).

41. D. Van Der Spoel, *et al.*, GROMACS: Fast, flexible, and free. *J Comput Chem* **26**, 1701–1718 (2005).

42. A. P. Thompson, *et al.*, LAMMPS - a flexible simulation tool for particle-based materials modeling at the atomic, meso, and continuum scales. *Computer Physics Communications* **271**, 108171 (2022).

Figures and Tables

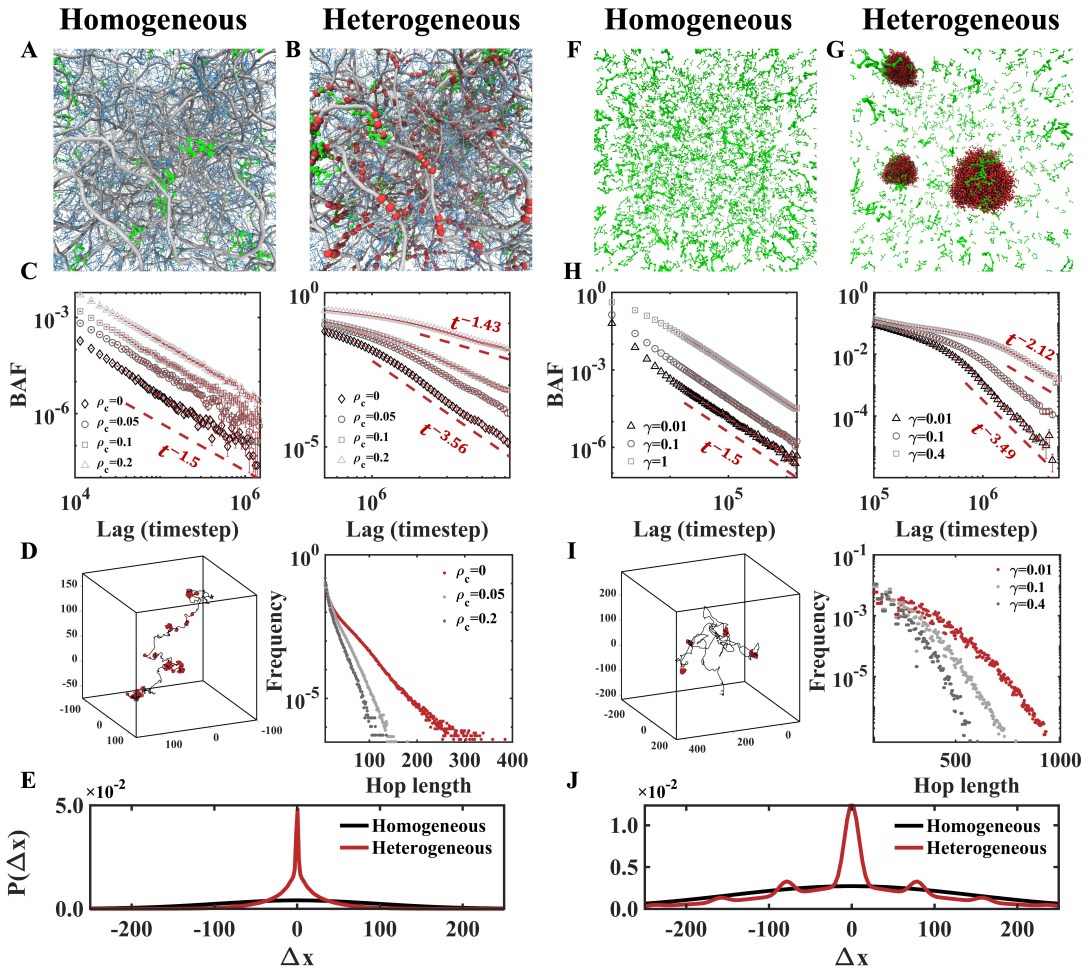

Fig. 1 **Comparison of binding dynamics in heterogeneous and homogeneous 3D binding systems. (A)** Simulation snapshot of protein polymers interacting with a long chromatin fiber in 3D, with non-specific interactions only. **(B)** Corresponding system configuration with 30% specific binding sites (red beads) interspersed along the chromatin fiber (gray). Crowding agents are shown as blue lines. **(C)** Binding autocorrelation functions (BAFs) under varying crowding conditions for the homogeneous system (left) and the heterogeneous one (right). The BAF in the heterogeneous system shows strong crowding-dependent regulation, unlike the homogeneous counterpart. **(D, Left)** A representative single-molecule trajectory in the heterogeneous system, showing hopping dynamics. Prolonged residence at binding sites is marked by red dots. **(D, Right)** Corresponding frequency distribution of hop lengths. **(E)** Displacement probability distributions (PDF) for heterogeneous and homogeneous systems, revealing non-Gaussian dynamics in the heterogeneous case. **(F, G)** Simulation snapshots of systems without and with liquid-liquid phase separation (LLPS), respectively. **(H)** BAFs for systems with and without LLPS. **(I, Left)** A representative molecular trajectory within the LLPS system. **(I, Right)** Frequency

distribution of hop lengths under LLPS conditions. **(J)** Comparison of PDFs in the presence and absence of LLPS.

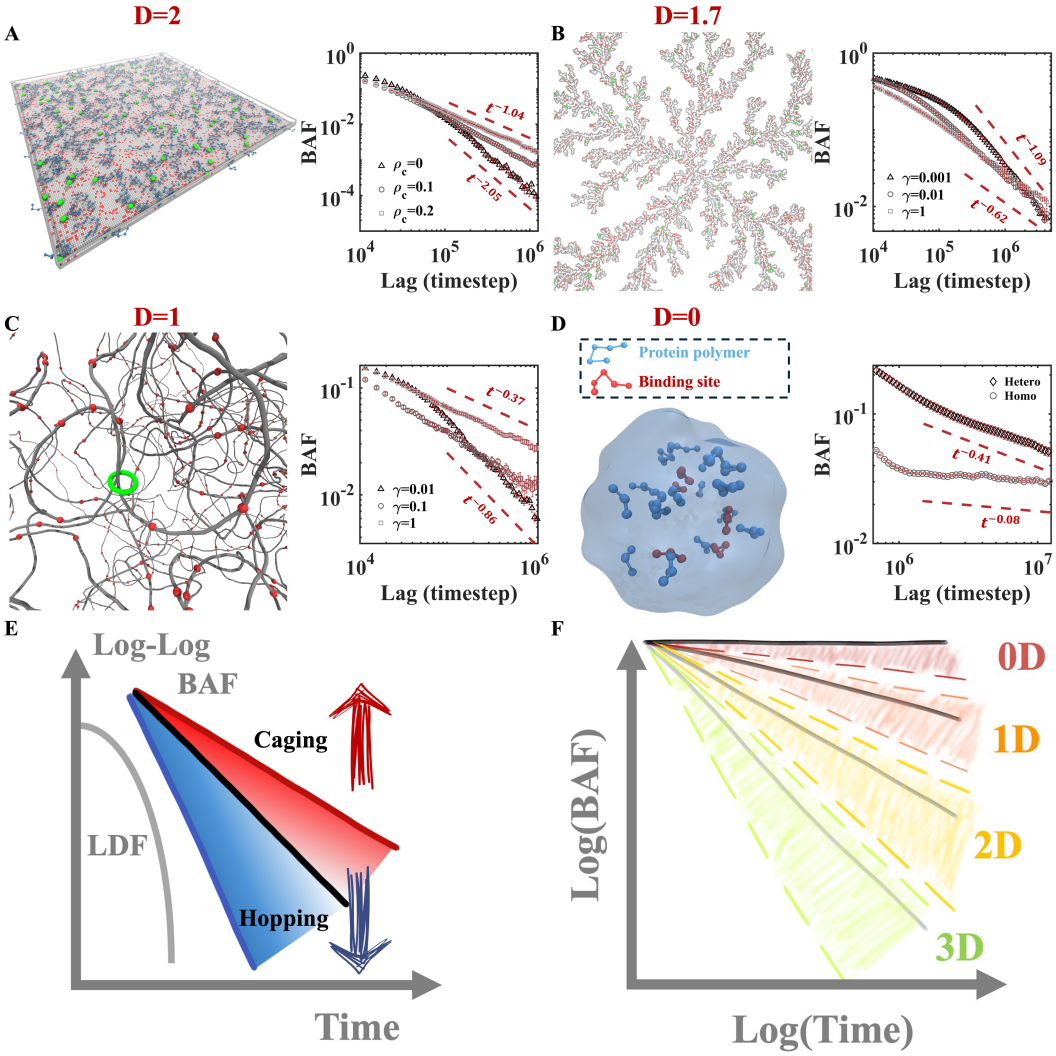

Fig 2. **Binding dynamics in low-dimensional heterogeneous systems. (A, Left)** Simulation snapshot of a 2D heterogeneous system with 10% specific binding sites (red). Adsorbed molecules and crowders are shown in green and blue, respectively. **(A, Right)** Corresponding BAF under varying crowding levels, showing crowding regulation. **(B, Left)** Schematic of a branched, fractal binding environment (D=1.7) generated via diffusion-limited aggregation. Here, 10% of the wall beads are functionalized as specific binding sites (green). **(B, Right)** BAF under varying solvent viscosities. **(C, Left)** Configuration of a ring polymer (green) undergoing facilitated sliding along a chromatin fiber (gray), where specific binding sites are marked as red dots. **(C, Right)** BAF as a function of solvent viscosity. **(D, Left)** Schematic of protein condensate (blue) with embedded specific sites (red). **(D, Right)** BAF measured in this quasi-zero-dimensional droplet environment, with and without specific binding sites. **(E)** Cartoon showing the bidirectional regulation of molecular binding memory through

hopping and caging mechanisms. **(F)** Cartoon: a rich spectrum of BAF scaling regimes emerge in low-dimensional heterogeneous environments.

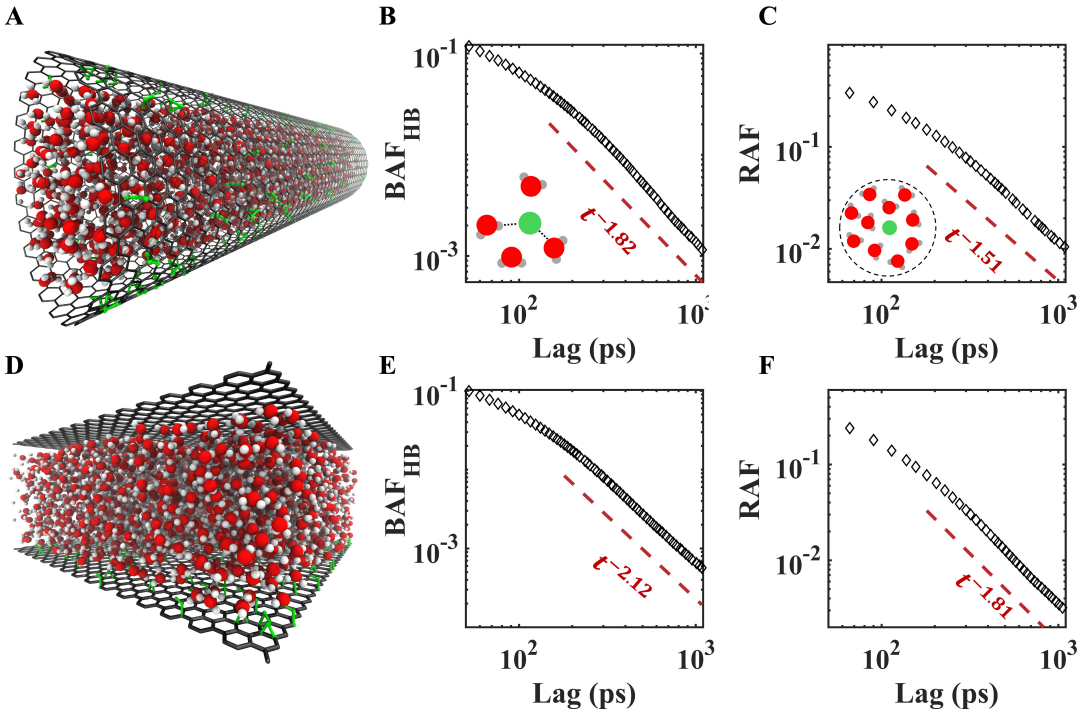

Fig 3. **All-atom simulations of water molecule dynamics in nanoconfined heterogeneous environments. (A)** Visualization of water molecules confined within a quasi-one-dimensional carbon nanotube (radius = 1.5 nm) functionalized with hydroxyl and epoxy groups at 5% surface coverage. **(B)** Binding autocorrelation function of hydrogen bonds formed between water molecules and the functional groups on the oxidized nanotube. **(C)** Residence time autocorrelation function for water molecules at specific adsorption sites (within 5 Å). **(D)** Simulation snapshot of water confined between two graphene layers (interlayer spacing d = 2.5 nm), forming a quasi-two-dimensional slit pore with 10% coverage of functional groups on the lower surface. **(E)** Corresponding hydrogen-bond BAF for the 2D case **(F)** Residence time autocorrelation for confined water in 2D. In all panels (B, C, E, F), power-law fits are shown as dashed lines with the corresponding scaling exponents indicated.

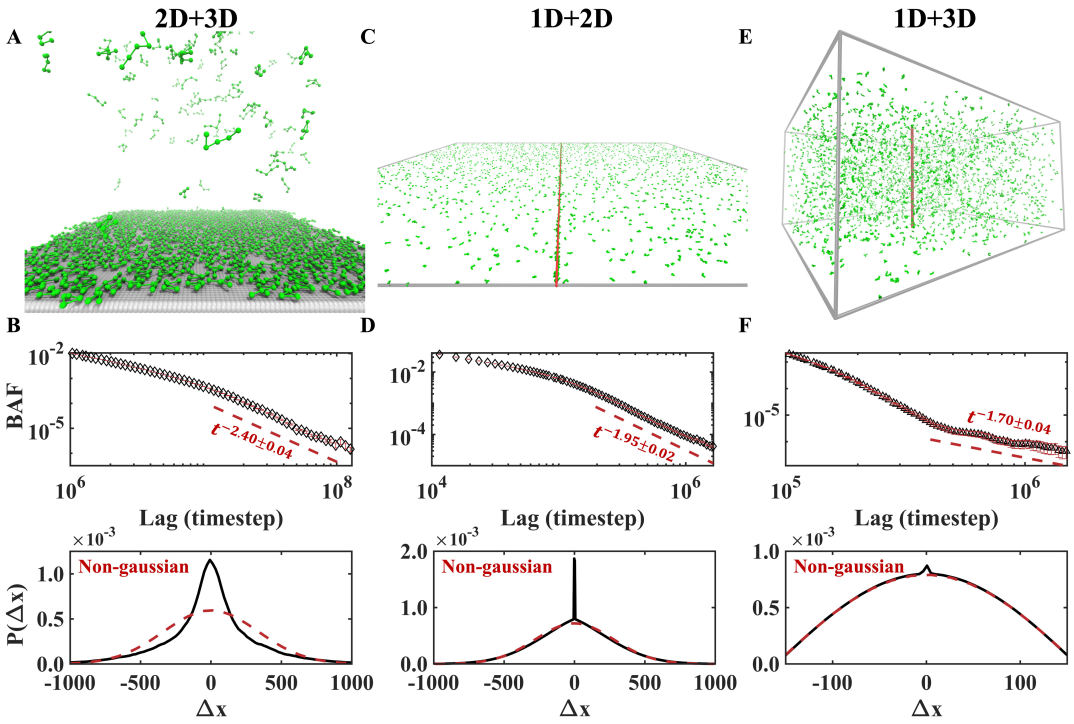

Fig. 4 **Binding dynamics in systems where heterogeneous binding sites are confined to a well-defined geometry. (A)** Schematic of molecular binding between 3D diffusing molecules and a 2D surface. **(B, Top)** Binding autocorrelation function measured for polymer-surface binding, revealing a universal $t^{-2.5}$ scaling. **(B, Bottom)** Non-Gaussian probability density function (PDF) of molecular displacements. The dashed line represents an attempted Gaussian fit. **(C, E)** Simulation snapshots of 2D and 3D diffusing molecules bound to a 1D polymer. **(D, F)** The identical analysis presented in (B) is applied to (D) 2D diffusing molecules specifically binding to a 1D array and (F) 3D diffusing molecules binding to a 1D linear array.

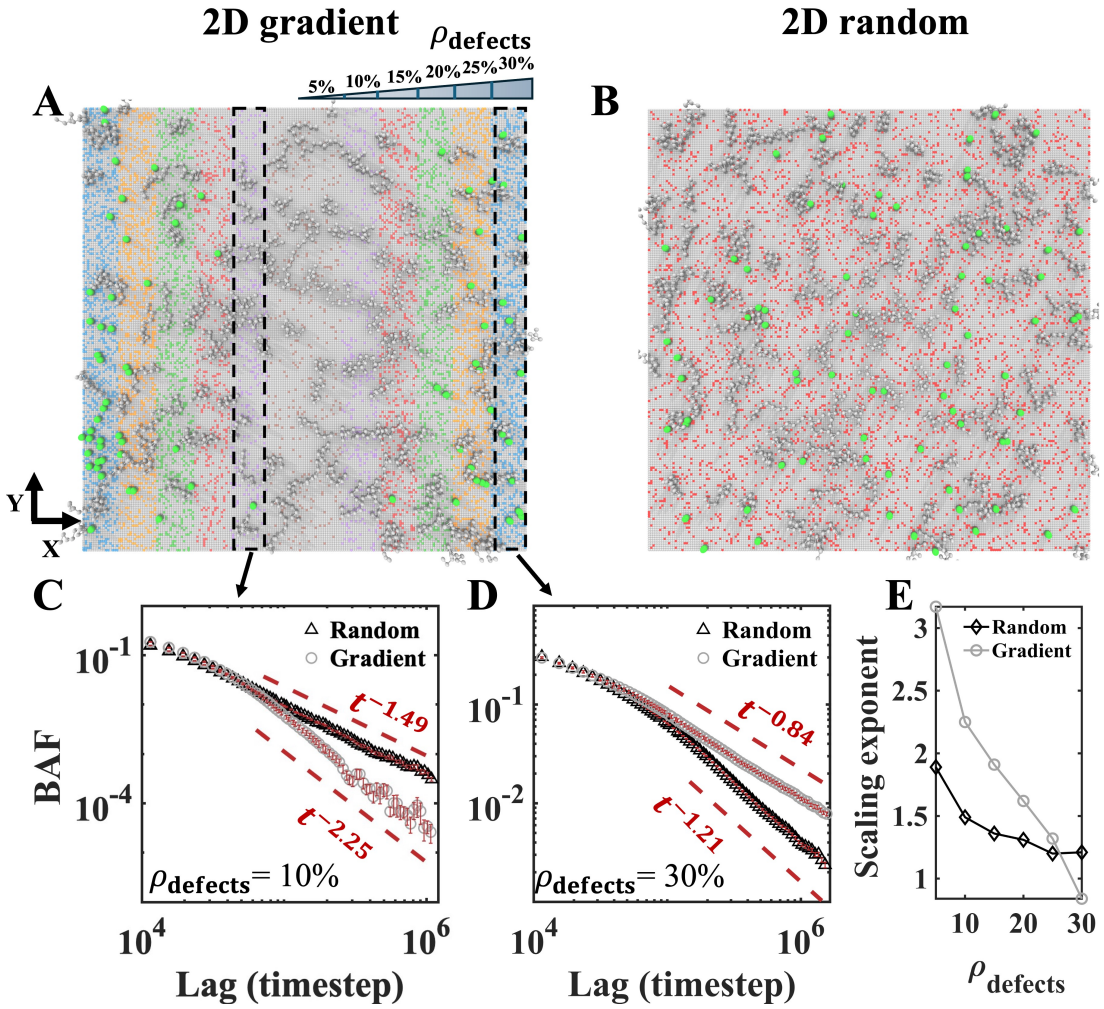

Fig. 5 **Molecular binding memory on surfaces with engineered binding gradients. (A)** Snapshot from molecular dynamics simulation, showing particle binding on a surface with a gradient of binding site density along the x-axis. **(B)** Schematic of the control surface with a random spatial distribution of binding sites. **(C, D)** Binding autocorrelation functions on the gradient-patterned surface compared to those random-patterned surfaces, at specific site densities of 10% (C) and 30% (D). **(E)** Scaling exponents derived from power-law fits to the BAFs, plotted as a function of specific site density for both surface patterns.

Supplementary Information

Anomalous binding memory in heterogeneous molecular systems

Shiyi Qin[1,†,*], Fangxuan Lyu[1,†], Xuebo Quan[1], Bing Miao[2], Kai Huang[1,*]

[1]Institute of Systems and Physical Biology, Shenzhen Bay Laboratory, Shenzhen, 518107, China

[2]Center of Materials Science and Optoelectronics Engineering, College of Materials Science and Opto-Electronic Technology, University of Chinese Academy of Sciences (UCAS), Beijing 100049, China

[†]These authors contribute equally

*Correspondence: qinsy@szbl.ac.cn (S.Q.), huangkai@szbl.ac.cn (K.H.)

The PDF file includes:

Supplementary Text

Supplementary Figures. 1 to 11

Protein polymer interacting with specific sites on chromatin fiber

Our molecular system was modeled in a 100×100×100 simulation box containing a chromatin fiber of 10000 beads and 250 protein polymers, each represented by a coarse-grained chain of 10 beads linked via harmonic bonds. Specific binding sites, defined as segments of three consecutive chromatin beads, were distributed along the fiber at 30% coverage. Non-specific interactions used a Lennard-Jones potentials with $\epsilon = 0.1$, while specific protein-site interactions used $\epsilon = 1.6$. The simulation ran for 1×10^7 steps, recording protein positions every 500 steps to track binding events.

Liquid-liquid phase separation droplet ensembles

To study a 3D heterogeneous binding environment formed by LLPS droplets, we simulated protein polymers in an 80×80×80 cubic simulation box with periodic boundary conditions in all dimensions. Each protein polymer, represented as a chain of 5 coarse-grained beads, had a number density of 0.005. Phase separation was induced by a strong polymer-polymer interaction strength of $\epsilon = 0.53$. The periodic boundaries effectively created a system of multiple droplets, each assigned a unique index for tracking. Over a total simulation of 5×10^6 steps, we recorded the center-of-mass positions of all polymers and droplets every 500 steps to analyze the probability of polymers rebinding to their original droplets.

2D confined heterogeneous system

We modeled the binding dynamics of 50 polymer chains in a quasi-2D geometry using a simulation box of dimensions 100×100×2.5. The polymers were placed above a functionalized substrate, modeled as a 200×200 array of beads, with 10% randomly selected as specific binding sites. Polymer-site interactions were governed by a Lennard-Jones potential ($\epsilon = 1.7$). Periodic boundary conditions were applied in the x and y directions to mimic an infinite plane, while confinement in the z direction restricted motion, enforcing quasi-2D behavior. The simulation was run for 5×10^6 steps, and the center-of-mass positions of all polymers were recorded every 500 steps for trajectory analysis.

Fractal heterogeneous binding system

To explore particle binding dynamics in fractal settings, we created diffusion-limited aggregation (DLA) generated branched structures through random walks. The void spaces within these structures were filled with immobile wall particles, after which the original DLA template was removed to yield a porous scaffold with a well-defined fractal dimension. Within this environment, 200 mobile adsorbate particles interacted weakly with each other via a Lennard-Jones potentials ($\epsilon = 0.15$) and experienced

steric repulsion from walls. Strong, specific binding was introduced by assigning 5% of the wall particles randomly with a high interaction strength ($\epsilon = 3.5$). The system was simulated using Langevin dynamics for 5×10^6 timesteps, and particle positions were sampled every 500 timesteps to analyze the binding kinetics.

1D heterogeneous binding system

We modeled the interaction between a ring polymer and a chromatin fiber within a 400×400×400 simulation box. The ring polymer, composed of 50 beads, was initially configured as a circle of fixed radius 3 and wrapped around a flexible chromatin fiber comprising 20000 beads. The chromatin fiber is represented as a flexible polymer, with harmonic bonding $U_b(\mathbf{r}) = 70(r - r_0)^2$ $(r_0 = 1)$ and a bending potential, $U_a(\mathbf{r}) = 5(\theta - \theta_0)^2$ $(\theta_0 = 180)$. To introduce binding specificity, 5% of the chromatin beads were randomly selected as high-affinity sites for the ring polymer, interacting with the ring with a Lennard-Jones potential with strength $\epsilon = 0.65$. Interactions between the ring and the remaining non-specific chromatin beads were weaker ($\epsilon = 0.05$). The system was equilibrated and evolved using Langevin dynamics for 2×10^6 steps. The positions of the ring and all binding sites were recorded every 500 steps to analyze binding and sliding dynamics, with the ring's position monitored to ensure it remained constrained to the fiber.

Binding dynamics of molecules within LLPS droplets

To confine protein polymers within LLPS droplets and establish a quasi-0D environment, we set interaction strength between protein polymers to $\epsilon = 0.75$. This strong LLPS ability ensured the dilute phase concentration was negligible, effectively suppressing exchange between the dense droplets and the surrounding medium. Heterogeneous binding within the droplets was introduced via six scaffold polymers (each a 5-bead chain, matching the protein polymer length), which served as specific high-affinity binding sites ($\epsilon = 1.25$). Binding dynamics were analyzed from particle trajectories recorded every 500 timesteps over a total simulation time of 10^7 timesteps.

All-atom molecular dynamics simulations of confined water

Water dynamics under nanoscale confinement were studied using all-atom MD. In the 1D system, water was confined within a single-walled oxidized carbon nanotube, restricting motion along the *z*-axis. An armchair (21,21) carbon nanotube (diameter 3 nm, length ~50 nm) was generated using an in-house MATLAB script. The structure was generated by replicating the translational unit cell along the tube axis, with duplicate atoms at periodic boundaries removed. To mimic internal surface oxidation, hydroxyl (-OH) and bridging epoxy (-O-) groups were randomly grafted onto the inner wall, each at a density of ~2.5% of the total carbon atoms, maintaining a minimum

inter-group distance of 4 Å. For the two-dimensional (2D) system, water was confined between two parallel graphene oxide sheets (30.3 × 31.5 × 2.0 nm³), with periodic boundaries in *x* and *y* to model an infinite slab. The OPLS-AA force field was used for the graphene oxide (GRO) and oxidized carbon nanotubes, and water was modeled with SPC/E. All simulations were conducted using GROMACS 2023.3. Each system was energy-minimized for 5000 steps and subsequently equilibrated in the NVT ensemble for 100 ps. Production simulations were then run for 40 ns. The leap-frog algorithm integrated the equations of motion with a 2-fs time step. Temperature was maintained at 300 K using the Nosé–Hoover thermostat with a 1.0 ps coupling constant. Non-bonded interactions were treated with a 1.2 nm real-space cutoff, applying a switch function for van der Waals potentials between 1.0 and 1.2 nm. Long-range electrostatics were handled by the Particle-Mesh Ewald method, and all bonds involving hydrogen were constrained using LINCS.

Heterogeneous binding systems of mixed dimensions

A. Binding of polymers with 2D solid surfaces in 3D bulk (2D+3D)

A 2D solid plane was constructed in a simulation box of dimensions 60×60×500 by placing immobile beads at 0.5 intervals along the *x*- and *y*- axes at *z*=0. Periodic boundary conditions in *x* and *y* created an infinite plane. The adsorbate polymers were coarse-grained 5-bead chains connected by harmonic springs $U_b(\mathbf{r}) = k(r - r_0)^2$ with a spring constant k =70 and an equilibrium bond length $r_0 = 1$. Non-bonded isotropic interactions between monomers were described by the standard 12-6 Lennard-Jones (LJ) potential, $U_{ij} = 4\epsilon\left[\left(\frac{\sigma}{r}\right)^{12} - \left(\frac{\sigma}{r}\right)^{6}\right]$, with the well depth ϵ varied to represent different binding affinities. The polymer concentration was fixed at 0.002, and the system was simulated for 1.5×10^8 steps, with the center-of-mass positions of all polymers recorded every 1000 steps to track surface binding.

B. Interactions of polymers with 1D chains in 2D and 3D bulk (1D+2D/2D+3D)

We studied binding dynamics in systems where specific interaction sites are strictly confined to a one-dimensional substrate embedded within higher-dimensional space (2D and 3D). In the 1D+2D system, a linear chain of binding sites was constructed along the *x*-axis in a 1000×1000×2 box, with periodic boundaries in *x* and *y* and reflective walls in *z* to enforce planar confinement. The affinity between the 1D solid chain surface and adsorbing molecules was set to $\epsilon = 0.5$. For the 1D chain embedded in 3D space (1D+3D), the chain was positioned at the center of the *x*-*y* plane and extended along the entire z-axis. The specific binding strength is set as $\epsilon = 0.75$. Both

systems were simulated for a total of 4×10^6 timesteps, with binding states sampled every 500 timesteps.

Simplified theory analysis

A. Analysis of BAF limits in mixed 2D and 3D environments

When we study the binding dynamics between polymers and a 2D adsorbing surface, we can use a 3D Fokker-Planck equation with absorbing boundary conditions to determine the limiting value of the binding autocorrelation function in the system:

$$\frac{\partial P(x,y,z,t)}{\partial t} = D\left(\frac{\partial^2 P}{\partial x^2} + \frac{\partial^2 P}{\partial y^2} + \frac{\partial^2 P}{\partial z^2}\right)$$

$$IC: P(x,y,z,0) = \delta(x)\delta(y)\delta(z-z_0)$$
$$BC: P(x,y,z=0,t) = 0$$

The solution was obtained via the method of images, combining the free diffusion Green's function with a negative mirror source:

$$G(x,y,z,t;z_0) = \frac{1}{(4\pi Dt)^{3/2}} \exp\left(-\frac{x^2+y^2+(z-z_0)^2}{4Dt}\right)$$

$$P(x,y,z,t) = G(x,y,z,t;z_0) - G(x,y,z,t;-z_0)$$

This simplifies to the leading-order long-time asymptotic form:

$$\begin{aligned} P(x,y,z,t) \approx & \frac{1}{(4\pi Dt)^{\frac{3}{2}}}\left(1 - \frac{x^2+y^2+(z-z_0)^2}{4Dt}\right) \\ & - \frac{1}{(4\pi Dt)^{\frac{3}{2}}}\left(1 - \frac{x^2+y^2+(z+z_0)^2}{4Dt}\right) \\ & = \frac{1}{(4\pi Dt)^{\frac{3}{2}}}\left(\frac{x^2+y^2+(z-z_0)^2}{4Dt} - \frac{x^2+y^2+(z+z_0)^2}{4Dt}\right) \\ & = \frac{1}{(4\pi Dt)^{\frac{3}{2}}}\frac{zz_0}{Dt} = \frac{zz_0}{(4\pi D)^{\frac{3}{2}}t^{\frac{5}{2}}} \end{aligned}$$

The time-dependent rebinding probability, defined as the survival probability within a cutoff distance r_c from the desorption site, is then obtained by integrating $P(x,y,z,t)$ over a hemispherical interaction volume:

$$P_{rebind}(t) \approx \int_0^{r_c}\int_0^{2\pi}\int_0^{\frac{\pi}{2}} \frac{rcos\theta z_0}{(4\pi D)^{\frac{3}{2}}t^{\frac{5}{2}}} r^2 sin\theta d\theta d\phi dr = \frac{z_0}{(4\pi D)^{\frac{3}{2}}t^{\frac{5}{2}}}\frac{r_c^4\pi}{4} \sim t^{-\frac{5}{2}}$$

B. Analysis of BAF limits in mixed 1D and 2D environments

The extreme scaling of the BAF for polymers interacting with a 1D adsorptive chain in a 2D space was determined by solving the following simplified problem:

$$\frac{\partial P(x,y,z,t)}{\partial t} = D\left(\frac{\partial^2 P}{\partial x^2} + \frac{\partial^2 P}{\partial y^2}\right)$$

with initial condition $P(x,y,z,0) = \delta(x)\delta(y-y_0)$ and an absorbing boundary condition at the chain location $P(x,y=0,t) = 0$. Using the method of images, the solution is constructed as:

$$P(x,y,t) = G(x,y,t;y_0) - G(x,y,t;-y_0)$$

where $G(x,y,z,t;z_0) = \frac{1}{(4\pi Dt)^{3/2}} \exp\left(-\frac{x^2+(y-y_0)^2}{4Dt}\right)$ is free-space Green's function in 2D. For small distances and long times, we approximate the exponential terms using $e^{-u} \approx 1-u$ for small u:

$$\exp\left(-\frac{x^2+(y-y_0)^2}{4Dt}\right) \approx 1 - \frac{x^2+(y-y_0)^2}{4Dt}$$

$$\exp\left(-\frac{x^2+(y+y_0)^2}{4Dt}\right) \approx 1 - \frac{x^2+(y+y_0)^2}{4Dt}$$

Thus:

$$P(x,y,t) \approx \frac{1}{4\pi Dt}\left[\left(1 - \frac{x^2+(y-y_0)^2}{4Dt}\right) - \left(1 - \frac{x^2+(y+y_0)^2}{4Dt}\right)\right]$$

$$= \frac{1}{4\pi Dt}\left[\frac{x^2+(y+y_0)^2 - x^2 - (y-y_0)^2}{4Dt}\right]$$

$$= \frac{1}{4\pi Dt}\left[\frac{(y+y_0)^2-(y-y_0)^2}{4Dt}\right] = \frac{1}{4\pi Dt}\left[\frac{(y^2+2yy_0+y_0^2)-(y^2-2yy_0+y_0^2)}{4Dt}\right]$$

$$= \frac{1}{4\pi Dt}\cdot\frac{4yy_0}{4Dt} = \frac{yy_0}{4\pi D^2t^2}$$

We integrate over a semicircular interaction range around the origin in the upper half-plane ($y \geq 0$) with radius r_c, using polar coordinates where $x = r\cos\theta$, $y = r\sin\theta$:

$$P_{\text{rebind}}(t) \approx \int_0^{r_c}\int_0^{\pi} \frac{(r\sin\theta)y_0}{4\pi D^2t^2} r\, dr\, d\theta$$

$$= \frac{y_0}{4\pi D^2t^2}\int_0^{r_c} r^2\, dr \int_0^{\pi} \sin\theta\, d\theta \sim t^{-2}$$

C. Numerical Modeling of BAF limits in mixed 1D and 3D environments

We modeled the rebinding dynamics of a molecule to a 1D absorbing polymer in 3D space by solving the azimuthally symmetric Fokker-Planck equation in cylindrical coordinates:

$$\frac{\partial P(r,z,t)}{\partial t} = D\left(\frac{\partial^2 P}{\partial r^2} + \frac{1}{r}\frac{\partial P}{\partial r} + \frac{\partial^2 P}{\partial z^2}\right)$$

with initial condition:

$$P(r,z,0) = \delta(r-r_0)\delta(z)$$

corresponding to a molecule initially desorbed at a small radial distance r_0 from the polymer axis at $r = 0$. The polymer was treated as a perfectly absorbing line (a strong

sink) at $r = 0$, enforced by $P(r = 0, z, t) = 0$. The rebinding probability is quantified by computing the time-dependent survival of the molecule within a cutoff radius r_c from its starting location.

The equation was solved using an explicit finite-difference scheme on a uniform grid with $N_r = N_z = 5000$points, spatial steps $\Delta r = \Delta z = 0.1$, and time step $\Delta t = 0.05$ (satisfying the stability criterion $\Delta t \leq 1/[2D(\Delta r^{-2} + \Delta z^{-2})]$ for $D = 10^{-3}$). The radial coordinate was discretized as $r_i = (i - 1)\Delta r$ $(i = 1, \ldots, N_r)$ and the axial coordinate as $z_j = (j - Nz/2 - 0.5)\Delta z$ $(j = 1, \ldots, N_z)$, with the probability density $P_{i,j}^n \approx P(r_i, z_j, t_n)$. Spatial derivatives were discretized using central differences:

$$\frac{\partial^2 P}{\partial r^2} \to \frac{P_{i+1,j} - 2P_{i,j} + P_{i-1,j}}{\Delta r^2}$$

$$\frac{1}{r}\frac{\partial P}{\partial r} \to \frac{1}{r_i}\frac{P_{i+1,j} - P_{i-1,j}}{2\Delta r}$$

$$\frac{\partial^2 P}{\partial z^2} \to \frac{P_{i,j+1} - 2P_{i,j} + P_{i,j-1}}{\Delta z^2}$$

applied at the interior points $2 \leq i \leq N_r - 1$, $2 \leq j \leq N_z - 1$. Time integration was performed via the forward Euler method:

$$P_{n+1} = P_n + \Delta t \cdot D\mathcal{L}[P^n]$$

where $\mathcal{L}$ is the discretized diffusion operator. The computation was parallelized over the (*i*,*j*) grid using OpenMP. Boundary conditions are imposed as:

$$P_{1,j} = 0 \text{ at r=0}$$

$$P_{N_r,j} = P_{N_{r-1},j} \text{ at } r_{max}$$

$$P_{i,1} = P_{i,2}, P_{i,N_z} = P_{i,N_{z-1}}$$

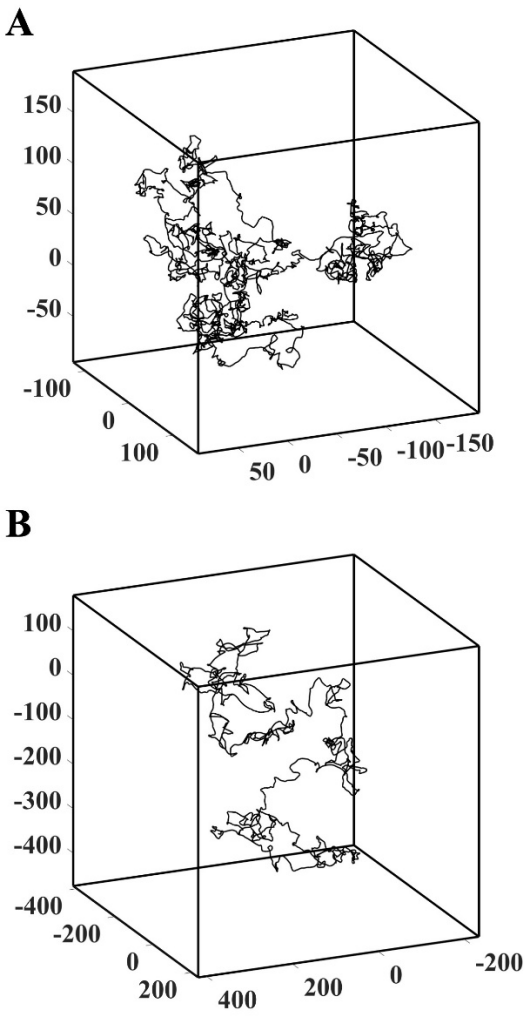

Fig. S1 Representative single-molecule trajectories in (A) polymers interacting non-specifically with chromatin fibers and (B) a homogeneous phase without phase separation.

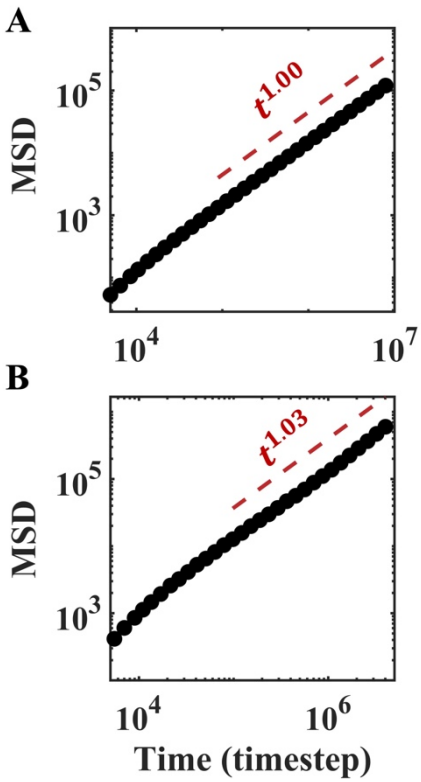

Fig. S2 Mean-squared displacement (MSD) of diffusing polymers in a TAF-chromatin binding system (A) and a liquid-liquid phase separation (LLPS) system (B). Power-law fits to the MSD curves are shown as red dashed lines.

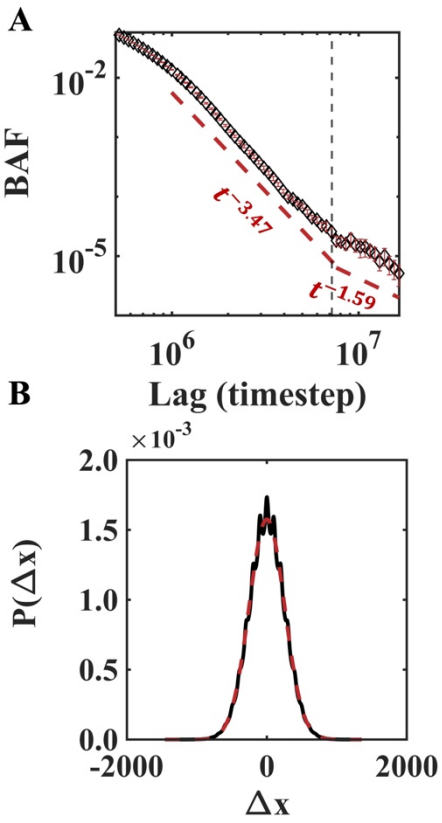

Fig. S3 (A) Binding autocorrelation function for protein polymers interacting with randomly distributed specific binding sites on chromatin. Compared with the simulation in Fig. 1, the duration was extended to 2×10^7. A clear scaling transition is observed at $t = 7.2 \times 10^6$ (indicated by the dashed line). Power-law fits to the two distinct temporal regimes are indicated by red dashed lines. (B) Displacement probability distribution function (PDF) for the protein polymers, computed at $\Delta t = 1.25 \times 10^7$. A Gaussian fit to the distribution is indicated by the red dashed line.

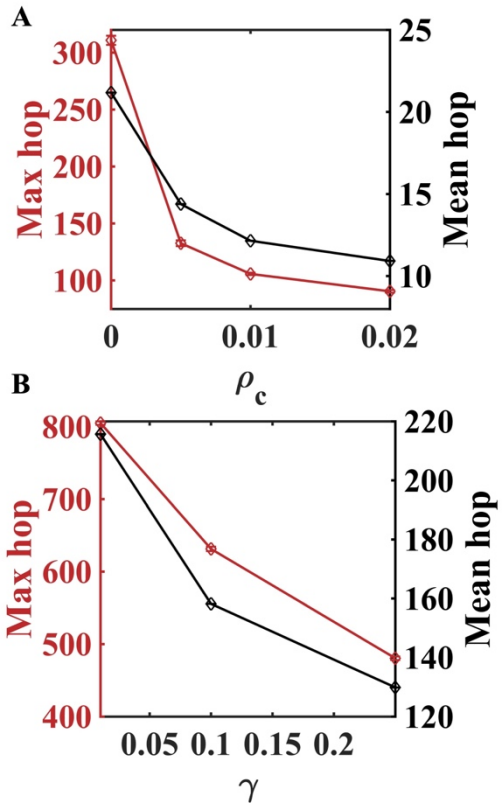

Fig. S4 Statistics of maximum and mean hop lengths for polymers in a TAF-chromatin interaction system (A) and a liquid-liquid phase separation (LLPS) system (B).

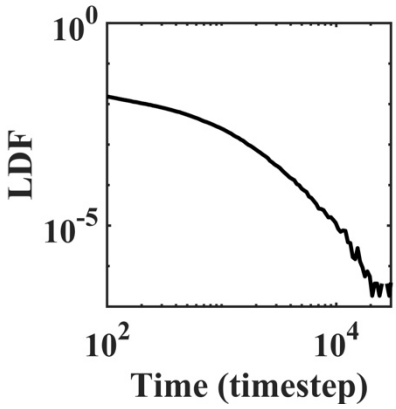

Fig. S5 Binding lifetime distribution analysis for protein polymers interacting with a long chromatin fiber with 30% specific binding sites.

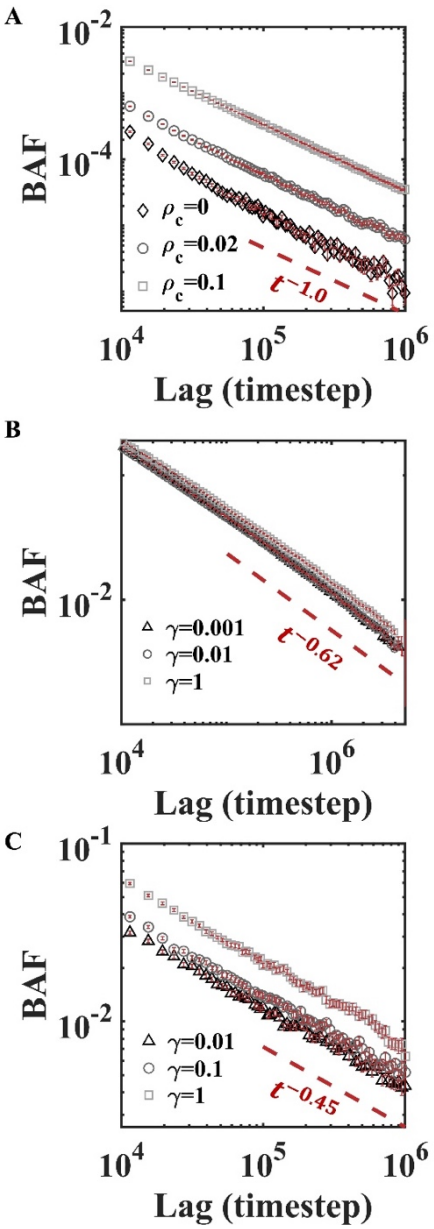

Fig. S6 Binding autocorrelation functions in homogeneous counterparts (nonspecific interactions only) of low-dimensional systems. Data are shown for systems of different dimensionalities: (A) 2D, (B) fractal (D = 1.7), and (C) 1D. For each system, BAF are measured under varying diffusion conditions, with fitted scaling laws indicated by red dashed lines.

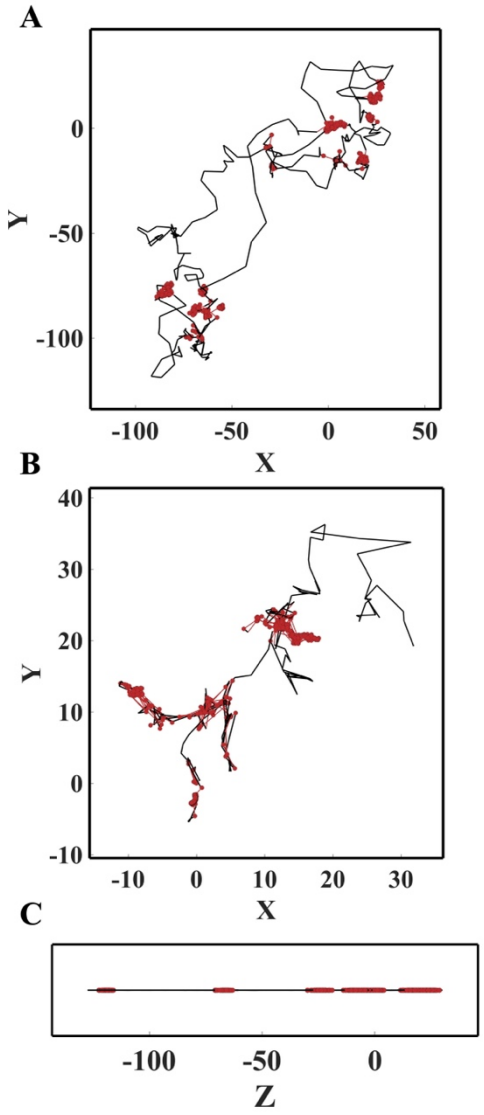

Fig. S7 Representative single-molecule trajectories in a confined quasi-2D system (A), a fractal system (B), and a 1D system (C), each with embedded specific binding sites. Red dots indicate regions of high trajectory density corresponding to molecular trapping events.

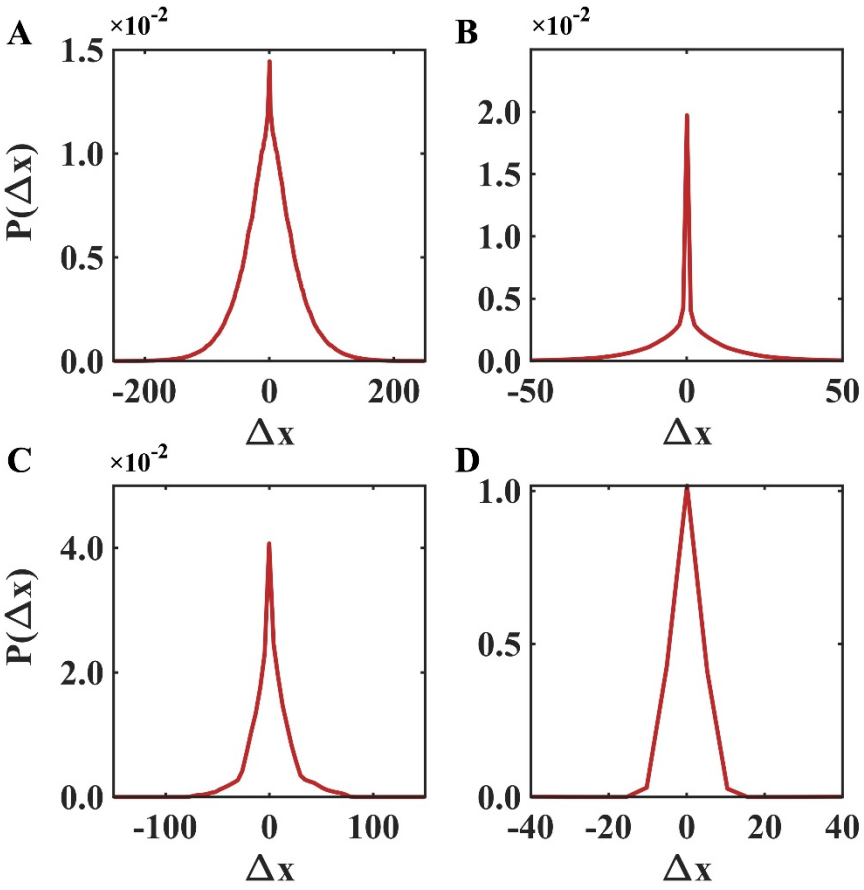

Fig. S8 Probability distribution functions of molecular displacement for heterogeneous binding systems in different dimensions: (A) 2D, (B) fractal (D = 1.7), (C) 1D, and (D) 0D.

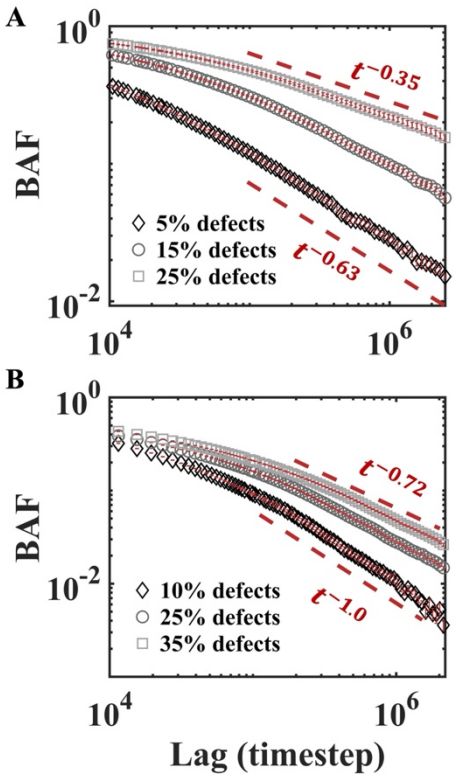

Fig. S9 Analysis of the binding autocorrelation function in (A) fractal and (B) 2D heterogeneous binding systems with varying proportions of binding defects. All simulations employ slow diffusion to suppress the hopping of single-bead binders. As the density of specific binding sites increases, adsorbed molecules experience enhanced local trapping, causing the BAF to drop below the homogeneous scaling baseline.

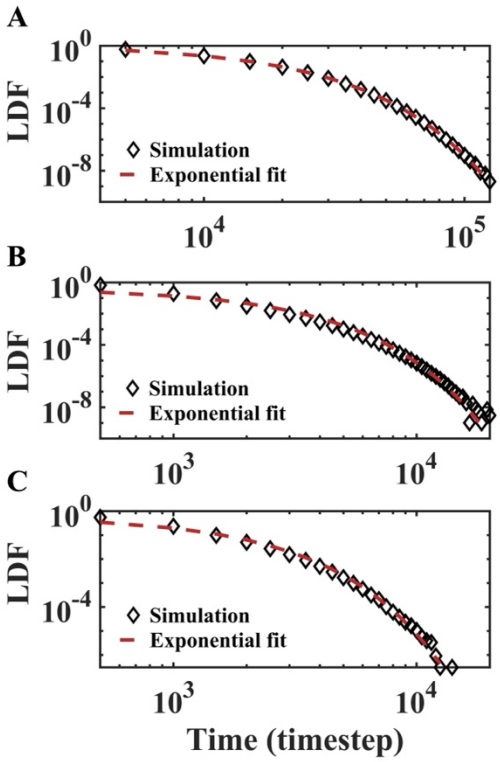

Fig. S10 Distribution of continuous binding residence times in mixed-dimensionality systems: (A) 2D + 3D, (B) 1D + 2D, and (C) 1D + 3D. All distributions are well described by single-exponential decay (red dashed lines).

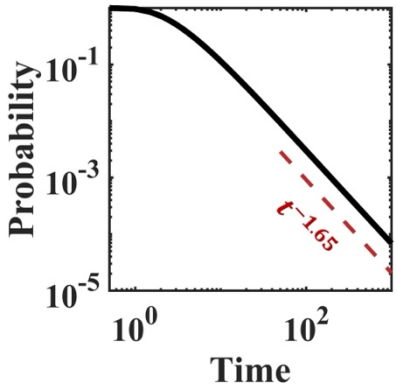

Fig. S11 Probability of a molecule rebinding to the original site on a one-dimensional chain with perfectly absorbing boundaries, corresponding to the no-return limiting case of single hopping. A power-law fit to the data is shown by the dashed line.